Polymer Testing, Volume 73, February 2019, Pages 338-345
DOI:10.1016/j.polymertesting.2018.11.034

Thermomechanical characterisation of cross-linked β-cyclodextrin polyether binders

Federico Luppi, Guillaume Kister, Mark Carpenter, Eleftheria Dossi*

Centre for Defence Chemistry, Cranfield University, Defence Academy of the United Kingdom, Shrivenham, SN6 8LA, UK

* Corresponding author: E-mail address: e.dossi@cranfield.ac.uk (E. Dossi).

Abstract

Cyclodextrins are promising building blocks for the synthesis of industrial binders. We determined the thermomechanical properties of a new binder prepared by cross-linking β-cyclodextrin with a variable amount of polyethylene glycol diglycidyl ether (40–60% w/w) to produce a soft polyether network that was soluble in water and alcohol. Increasing the amount of cross-linker reduced the glass transition temperature of the binder as determined by differential scanning calorimetry and dynamic mechanical analysis. Cooling experiments revealed sudden stress relief below the glass transition temperature, reflecting the de-bonding of the polymer from the metallic supports. This was prevented by contact with polytetrafluoroethylene tape. Optical microscopy confirmed the stress relief in the form of cracking and revealed self-healing by reptation, promoted by a higher cross-linker content and temperature. The influence of the support medium on the thermomechanical properties of the cross-linked β-cyclodextrins will help to optimise manufacturing and storage methods for new binders.

Keywords: differential scanning calorimetry, dynamic mechanical analysis, polyethylene glycol, processability, self-healing, adhesiveness

1 Introduction

Binders are typically large molecules that are used to bond the ingredients in formulations and improve the physicochemical properties of the mixture. The paint manufacturing industry is historically one of the major investors in the development of new polymeric binders in order to improve the cohesion of pigment particles and adhesion to the coated substrate following evaporation of the solvent [1–3]. The electronics industry uses binders to improve the conductivity and mechanical strength of electrodes in batteries [4–6]. Binders are also used in rocket manufacturing to improve the safety and ballistic performance of propellants [7,8]. Finally, medical researchers seek biocompatible binders that facilitate controlled drug release [9]. Most current binders are derived from petrochemical resources and there is a strong demand for more sustainable alternatives [4,10–12].

Cyclodextrins (CDs) are polysaccharides derived from starch that provide a promising set of sustainable building blocks for the synthesis of new binders, particularly in the pharmaceutical industry [14]. As shown in Fig. 1, these toroidal macrocycles comprise six, seven or eight glucopyranose units to form α, β and γ CDs, respectively [14]. CDs have the ability to complex small molecules and alter their physicochemical properties, allowing the controlled release of drugs [15,16] or the entrapment and inactivation of toxins [17]. The many hydroxyl groups carried by CDs are easily derivatised to yield binders that can be used to manufacture electrodes [18–20] or drug products [21–24]. Polymeric derivatives of all three types of CDs can respond to external stimuli such as pH or temperature and safely deliver their cargoes of drugs to target organs [25–27]. In order to process the encapsulated drugs, crystalline CDs have been chemically modified to allow the incorporation of drugs during extrusion [26–28]. CDs were cross-linked with either multifunctional isocyanate or ethylene glycol diepoxides to form insoluble hydrogels, which can easily be formulated into pills or capsules [15,29–32]. These hydrogels are thermoresponsive and some of them self-heal following physical damage [31,33]. The self-healing mechanism relies on the supramolecular interactions in the hydrogel such as hydrogen bonding promoted by the hydroxyl groups in the polymer [34] and interactions between CD macrocycles and the polyether chains [35–37]. Furthermore, the soft hydrogel matrix allows the polymer chains to diffuse and re-bond in a damaged area [38–40]. The self-repair of damaged synthetic materials typically involves physical flow of the material at or near the damaged area followed by reversible covalent bonding or supramolecular chemistry, which also includes metal-ligand coordination, π-π stacking and ionic interactions [41].

Most self-repairing CD systems show a high degree of cross-linking and are insoluble in water and common organic solvents. This limits their use as binders because post-synthesis reactions cannot be achieved without

modifying the chemical structure, and the hydrogel becomes brittle because it cannot dissipate mechanical stress when swollen [42]. To address these drawbacks, we recently synthesised water and alcohol soluble cross-linked βCDs using polyethylene glycol diglycidyl ether (βCPCDs) [13]. Here, we characterised the thermomechanical properties of the cross-linked βCPCD system and investigated the thermosensitive, self-healing and adhesive behaviour of the synthetic materials by differential scanning calorimetry (DSC) and dynamic mechanical analysis (DMA). These experiments provide more information about these new binders and will facilitate the development of appropriate manufacturing and storage methods.

2 Materials

The βCPCD samples were synthesised from βCD (≥97% purity, Sigma-Aldrich) prepared as a stock (13% water content, determined by thermogravimetric analysis) and polyethylene glycol diglycidyl ether (PEGDGE, Sigma-Aldrich, Mw = 500 Da, polydispersity index = 1.7) as previously described [13]. The chemical structure and purity of all precursors and products were assessed by proton nuclear magnetic resonance (^{1}H-NMR) spectroscopy and DSC. The PEGDGE/βCD ratios we used are reported in Table 1, and the PEG/βCD ratio in the cross-linked products was determined by ^{1}H-NMR as previously described [35]. The physical appearance of the cross-linked products was influenced by the proportion of PEGDGE: cross-linked malleable products were generated when the PEGDGE content exceeded 50% w/w (Fig. 2a, sample βCPCD1), whereas powdery products were generated when less PEGDGE was present (Fig. 2b, sample βCPCD3).

3 Experimental

3.1 Dynamic mechanical analysis

The thermomechanical properties of the βCPCD products were determined by DMA using a Perkin Elmer DMA8000 device. The samples underwent a controlled sinusoidal displacement of 0.05 mm at frequencies of 1, 5 and 10 Hz in the single cantilever clamping bending configuration. The storage modulus (E′), loss modulus (E″) and damping factor (tanδ) were monitored as a function of temperature and time. The free sample length between the vibrating and fixed cantilever clamps was ~15 mm. The testing temperature was cycled up to three times between –100 and 140 °C at a rate of either 2 or 10 °C min^{-1}. Each material was tested in triplicate under each condition.

The cross-linked βCPCD samples were incapable of self-support, and were therefore tested in aluminium pockets (Fig. 3a), a stainless steel mesh (Fig. 3b), or aluminium pockets with polytetrafluoroethylene (PTFE)

tape (Fig. 3c) as recommended by Perkin Elmer. The aluminium pockets consisted of rectangular shims (30 x 14 mm) cut from a 0.1 mm thick aluminium strip (supplied by RS) and then folded lengthwise to form the pockets. We placed ~25 mg of the cross-linked βCPCD sample in the centre of each pocket. PTFE tape (30 x 15 mm) was used to fold the sample in the pocket and assess the bonding interaction between the sample and the metallic support during cooling. Rectangular strips of type 18 mesh (30 x 15 mm) were cut from a 0.65 mm thick sheet (supplied by RS). We spread ~30 mg of the crosslinked βCPCD material around and in the centre of the mesh strips.

3.2 Differential scanning calorimetry

Thermal analysis of the βCPCD samples and their precursors was carried out using a Mettler Toledo DSC3+ device. We placed 10 mg of the material in a 40 µl aluminium pan with a pierced lid. The DSC chamber was continuously purged with N_2 gas at a flow rate of 50 ml min^{-1}. The testing temperature was cycled three times between –100 and 140 °C. The variation of the heat flow in the samples was recorded as a function of temperature and time.

3.3 Optical microscopy

The dynamic physical properties of the βCPCD materials under the influence of temperature were investigated by optical microscopy using a Leica DM microscope fitted with a temperature-controlled stage (Linkam THMS 600). The temperature was changed using a T95 controller and an automated LNP95 liquid N_2 pump (both from Linkam). The material was placed on a 0.5 mm thick quartz microscopy cover slip. The slide was placed in a carrier within the stage to allow visual scanning. The stage was cooled to –100 °C and then heated to 100 °C at either 2 or 10 °C min^{-1}. To prevent condensation forming on the windows of the cold stage, the interior was purged with dry N_2 gas prior to cooling. A digital Qicam Fast 1394 CCD camera (QImaging) was used to continuously record any changes in the samples during the temperature cycle. The sample was illuminated by a white light source set in transmission mode.

4 Results and discussion

4.1 Precursor analysis – βCD

DMA was used to determine the storage modulus (E′) and damping factor (tanδ) of βCD over three heating/cooling cycles from –100 °C to 140 °C at 10 °C min^{-1}. The last cycle is shown in Fig. 4. The E′ value was slightly higher during the first thermal cycle compared to the second and third cycles, reflecting the presence of synthesis-dependent stresses. There were no significant differences between the second and third thermal cycles, which are shown in the Supporting Information (SI).

The E′ values of the pure βCD sample were inversely related to the temperature, whereas the tanδ values remained relatively constant during each temperature cycle, showing there was no phase transition. This is consistent with earlier experiments that defined βCD as a crystalline compound [14]. A minor hysteresis was observed between cooling and heating. The lower E′ value during heating reflects the higher degree of relaxation in the material at high temperatures. Therefore the higher E′ value during cooling is due to the stress created by the high cooling rate.

The variation in E′ and tanδ was also investigated as function of the oscillation frequency. The increase in frequency during the temperature cycle had no significant influence on either value. The corresponding thermogram is shown in the SI. A phase transition indicated by DSC at 83 °C (Fig. 5) persisted at temperature cycles up to 140 °C. Earlier reports attributed this phenomenon to the dissolution of βCD crystals in the water present in the sample [43]. Molecular dynamics simulations predicted a glass transition temperature (T_g) for βCD of 61 °C [44] whereas others reported a measured T_g value of 216 °C [45].

4.2 Precursor analysis – PEGDGE cross-linker

DMA was also used to determine the thermomechanical properties of the PEGDGE cross-linker, again with three heating/cooling cycles from –100 °C to 140 °C at 10 °C min^{-1}. There was no significant difference between the thermal cycles so only the third cycle is shown in Fig. 6. The E′ value fell during heating, with two main transitions at –70 °C and –22 °C corresponding to the glass transitions of the PEGDGE sample. The broad and laddered decline in E′ reflects the specific properties of this commercial product, a blend of polyethylene glycol (PEG) chains with an average molecular weight of 500 Da and a polydispersity index of 1.7.

Previous studies have shown that the T_g of PEGDGE is inversely related to its polydispersity because the shortest polymer chains act as a plasticiser, reducing the brittleness, lowering the tensile strength and increasing impact strength of the material overall [46,47]. During cooling, PEGDGE underwent a single glass transition event, increasing its stiffness. However, the rapid increase in E′ from about –30 °C was followed by

a sudden drop at about –75 °C, the latter corresponding to 28% of the maximum E′ value. This phenomenon also occurred in tests conducted at the lower heating/cooling rate of 2 °C min^{-1}. DMA was used to test the aluminium support in order to eliminate artefacts caused by the machine and/or support matrix (SI). The E′ value of the support showed linear variation within the experimental temperature range, suggesting that the observed phenomenon is caused by the viscoelastic behaviour of the PEGDGE and its strong interaction with the supporting pocket. Hydroxyl, epoxy and carboxyl functionalities in a polymer allow the formation of hydrogen bonds with metal and glass [48]. The strong adhesive interactions and the change in the stiffness of the PEGDGE sample during the glass transition promote internal stress which is suddenly released, initiating cracking and de-bonding of the sample from the support, recorded as a sudden drop in the E′ value. The physical damage (such as cracking) that emerged during the cooling cycle provided an interesting initial assessment of the adhesive strength between the sample and different support matrices. The same thermal profile during the second and third cycles confirmed that PEGDGE recovers its initial mechanical properties when heated above the T_g in each cycle, and the process is therefore reversible.

The effect of the oscillation frequency on the mechanical properties of PEGDGE was tested at 1, 5 and 10 Hz. The E′ curves at 1 and 10 Hz are shown in Fig. 7. The cooling and heating curves at both frequencies diverge at the point of glass transition. During heating, the glass transition of the compound is complete at ~25 °C as confirmed by the small decrease in E′ and the overlapping of the curves at different frequencies. The T_g is directly proportional to the frequency during both heating and cooling, and thus increases at higher frequencies [49,50]. The drop in the E′ values caused by cracking is also influenced by the oscillation frequency: the E′ peak at 1 and 5 Hz occurs at –78 °C whereas the 10 Hz peak occurs at –70 °C.

The cracking of the PEGDGE samples was analysed by DSC with a temperature cycle between –100 and 100 °C. The heat flow variation in the sample during the third temperature cycle is shown in Fig. 8. DSC revealed a thermal transition during the cooling interval from –23 to –50 °C reflecting both the crystallisation and vitrification of the blend. Therefore, the mechanical phenomenon observed by DMA is likely to occur when the PEGDGE becomes fragile following crystallisation of the longer chains (–34 °C) and vitrification of the shorter chains (–42 °C). The lower baseline heat flow adsorption after the crystallisation peak from –22 °C possibly indicates the presence of a glass transition due to the middle-length and shorter polymer chains that act as a plasticiser, as reported for PEG [51]. During heating, the heat flow adsorption of the PEGDGE increases between –70 and 10 °C in a multi-step transition that represents the combination of longer polymer chains melting (~1 °C) and the increased mobility of the middle length and shorter chains after the glass transition. Notably, the phase transformation measured by DMA occurred at a higher temperature compared

to that recorded by DSC (Table 1), probably reflecting the oscillation frequency applied to each sample and the different sample masses used in the two analytical techniques.

4.3 Analysis of the βCPCD product in aluminium pockets

The characteristics of the precursors allowed us to select suitable methods for the analysis of βCPCD product samples. First, we used DMA and DSC to determine how the amount of PEGDGE cross-linker (ranging from 40% to 60%) affected the thermomechanical properties of βCPCD, initially with the samples held in aluminium pockets as recommended for materials incapable of self-support. The DMA and DSC data for βCD, PEGDGE and βCPCD are compared in Table 1.

The E′ and tanδ values for βCPCD1 containing 60% PEG units during the third temperature cycle from –100 to 140 °C are shown in Fig. 9. There were no significant differences in either value when comparing the three temperature cycles, suggesting that the cross-linked system is not affected by the thermal history of the sample, as observed for PEGDGE (SI). The PEG chains dominated the behaviour of the cross-linked samples, with a notable shift in the transitions towards positive temperature values. During heating, DMA revealed a gradual stepwise decrease in E′ between the temperature extremes with a major step at 55 °C coinciding with a tanδ peak. This broad transition was frequency dependent, suggesting it represented a glass transition event for βCPCD1 (SI). The softening of the βCPCD1 product was represented by a change in the slope of the E′ curve at –10 °C, matching with the onset of the tanδ peak, and this relates to the viscoelasticity of the PEG soft segments.

With an aluminium support in place, the DMA thermogram for βCPCD1 showed a similar profile to PEGDGE during the cooling phase, which can be attributed to the cracking of the sample. A sudden drop in E′ from its maximum value to 31% occurs at around –42 °C. The temperature at which cracks begin to appear in the βCPCD1 sample was not significantly dependent on the oscillation frequency, whereas cracking of the PEG chains shifted from –78 °C at 1 Hz in PEGDGE to –70 °C at 10 Hz. The lower mobility of the βCPCD1 samples reflects the existence of a cross-linked matrix compared to the viscous PEGDGE liquid, which has a higher adhesive surface area.

The DMA curves of samples βCPCD1 (60% w/w PEGDGE) and βCPCD3 (40% w/w PEGDGE) are compared in Fig. 10. When the PEG content was lower, the βCPCD cracked at a much higher temperature (35 °C) and the E′ value dropped to 10% of its maximum, far below the 30% of maximum observed for the

sample with a higher PEG content. A low PEG content appears to increase the brittleness of the sample and reduces its viscoelastic behaviour, also reducing its binding strength given that the drop in E′ is related to the strength of adhesion to the metallic support. The glass transitions determined from the peak tanδ values shift to higher temperatures when the PEG content is low. The absence of first-order transitions in the βCPCD samples during cooling was confirmed by DSC (Fig. 11 and SI) suggesting that βCPCD products are completely amorphous at temperatures between –100 and 100 °C.

4.4 Analysis of the βCPCD product on a steel mesh support

We also investigated the way in which βCPCD1 (60% w/w PEGDGE) and βCPCD3 (40% w/w PEGDGE) interacted with a stainless-steel mesh in lieu of the aluminium pocket. The samples were spread over the mesh prior to analysis (Fig. 1b). The glass transition of βCPCD1 as determined by DMA was interrupted by stress relaxation at 15 °C (Fig. 12). The relaxation declined between the thermal cycles but was still present during the third cycle (SI). Cracking was still observed during cooling, but the phenomenon was less severe when compared to the sample held in an aluminium pocket (Fig. 12). The cracking also manifested itself over a wider temperature range (–14 °C to –70°C) compared to the sudden drop observed with the aluminium pocket. The characteristic drop in E′ began at about –17 °C and reached 3% of the maximum value. The drop was visible during each cycle, confirming the stress relaxation effect that occurs with each round of heating. The metallic mesh changes the manner in which the stress introduced during each cooling cycle is dissipated. The mesh has a greater surface area to which the βCPCD1 can bind (362 mm^2) compared to the aluminium pocket (180 mm^2) but nevertheless allows stress to be dissipated within the bulk sample much more effectively.

4.5 Analysis of the βCPCD product in aluminium pockets with PTFE tape

Finally, to confirm that the drop in the E′ values during cooling was due to the de-bonding of the sample from its support, we used PTFE tape to hold βCPCD1 samples within an aluminium pocket, thus allowing the samples to contract freely with the decreasing temperature. Preliminary DMA characterisation of the PTFE tape (blank) showed a softening at the onset temperature of 18 °C (SI). The absence of adhesion between βCPCD1 and the support when enclosed by PTFE tape was confirmed by the drop in E′ during cooling as shown in Fig. 13. The hysteresis between the heating and cooling curves during the same temperature cycle diminished with each cycle. Therefore, the PTFE tape almost completely eliminated the de-bonding

phenomenon and the formation of thermal stress in the sample during the cooling phase. The T_g of βCPCD1 under these conditions was 41°C, identical to the value recorded in the aluminium pocket without tape, confirming that the experimental setup does not affect the T_g.

4.6 Analysis of the βCPCD product by optical microscopy

We used optical microscopy to characterise in more detail the cracking that occurred in the βCPCD1 product during cooling (Fig. 14). A glass support was considered adequate as a transparent substitute for the metallic support we used to investigate the adhesion of the compound. The sample was cooled from 25 °C (Fig. 14a) and began to crack at about –55 °C (Fig. 14b), with the cracks propagating further as the temperature was reduced to –100 °C (Fig. 14c and 14d). The same sample was then heated to 100 °C and the cracks began to self-repair, starting at 0°C (Fig. 14e) until complete healing was observed at about 80 °C (Fig. 14h).

During a second thermal cycle on the same sample, cracking began at –58°C and initiated at a different location (Fig. 15c). This confirms the evidence provided by the similar E′ value profiles in each thermal cycle, i.e. the thermal history of the sample is erased by heating as previously reported for a hydrogel CD/PEG system [33]. In the second cycle, sample healing occurred at about 80 °C as in the first run (Fig. 15h). Furthermore, βCPCD1 placed on PTFE tape showed no evidence of cracking during the cooling phase, confirming that stress relief by cracking was due to the bonding of βCPCD1 to the glass support (SI).

This experiment confirmed the self-healing of the compound and explained why the E′ curves are identical during multiple temperature cycles. The self-healing behaviour is thought to reflect the reformation of hydrogen bonds and host–guest interactions as seen in CD hydrogel systems due to the reduction of the viscosity of the cross-linked system when heated above T_g [33,52–54]. The physical transformation occurs at the onset of material flow behaviour, allowing the crack to be filled in, and probably involves a rheological model involving the snake-like displacement of the polymeric chains, described as reptation [55].

The rupture strength of sample βCPCD1 was qualitatively assessed by intentionally cutting the sample (Fig. 16b). Both parts were subsequently re-joined and annealed in the oven at 70 °C for 30 min (Fig.16c). The joined parts were found to be cohesive after this qualitative test (Fig. 16d). The sample was gripped at its extremities and pulled gently. The sample showed considerable elongation. Diffusion of the polymeric chains by reptation and the reforming of hydrogen bonds in the fracture allowed the material to qualitatively self-

repair and self-heal. In future work, we will assess the self-healing capabilities of this compound in more detail.

5 Conclusions

The thermomechanical properties of a new cross-linked binder based on βCD and PEG segments were assessed by DSC and DMA. The cross-linking improved the processability of the material compared to crystalline βCD, which has unsuitable physical properties for a binder. All cross-linked βCPCD products showed viscoelastic responses similar to those observed for the pure cross-linker. The viscoelasticity was directly related to the proportion of cross-linker in the βCPCD system, with T_g values as low as –17 °C (determined by DSC) when cross-linker content was > 50% w/w. DMA revealed a sudden drop in E′ during the cooling sequence, and the amplitude of the drop was directly proportional to the amount of cross-linker present. This phenomenon is thought to reflect the de-bonding of βCPCD from the metallic support when the sample was cooled below T_g. The adhesiveness of the material was drastically reduced when folded in PTFE film indicating that the adhesive strength is due to the ability to form hydrogen bonds with the metallic support. Optical microscopy confirmed that the adhesiveness between the samples and the support, combined with the changes in viscoelasticity of the PEG and βCPCD segments at temperatures below T_g, produced mechanical stress that resulted in the propagation of cracks in the cross-linked material. Interestingly, the damaged βCPCD structure was able to restore its integrity by self-healing, which began at 0 °C and achieved complete self-repair at about 80 °C. The results show that the thermomechanical properties of the βCPCD system are superior to those of pure βCD. The influence of the support matrix on the thermomechanical properties of βCPCD could facilitate the development of optimal manufacturing and storage methods for new binders.

Funding

This project was funded through the Weapons Science and Technology Centre (WSTC) by the UK Defence Science and Technology Laboratory (DSTL).

Appendix A. Supplementary data

Supplementary data (SI) to this article can be found online at https://…..

References

[1] K.K. Sutna, S. Jacob, R. Joseph, Paint formulation using water based binder and property studies, Macromol. Symp. 277 (2009) 144–151. doi:10.1002/masy.200950318.

[2] F.F. Abdel-Mohsen, H.S. Emira, A study of the effects of different binders and fillers on the properties of flame retardant paints, Pigment Resin Technol. 36 (2007) 67–73. doi:10.1108/03699420710733493.

[3] V. Alvarez, M. Paulis, Effect of acrylic binder type and calcium carbonate filler amount on the properties of paint-like blends, Prog. Org. Coatings. 112 (2017) 210–218. doi:10.1016/j.porgcoat.2017.07.023.

[4] B. Andres, C. Dahlström, N. Blomquist, M. Norgren, H. Olin, Cellulose binders for electric double-layer capacitor electrodes: The influence of cellulose quality on electrical properties, Mater. Des. 141 (2018) 342–349. doi:10.1016/j.matdes.2017.12.041.

[5] D. Mazouzi, Z. Karkar, C.R. Hernandez, P.J. Manero, D. Guyomard, L. Roué, B. Lestriez, Critical roles of binders and formulation at multiscales of silicon-based composite electrodes, J. Power Sources. 280 (2015) 533–549. doi:10.1016/j.jpowsour.2015.01.140.

[6] J.E.S. Technol, N. Choi, S. Ha, Y. Lee, J.Y. Jang, M. Jeong, W.C. Shin, M. Ue, Recent Progress on Polymeric Binders for Silicon Anodes in Lithium-Ion Batteries, J. Electrochem. Sci. Technol. 6 (2015) 35–49. doi:10.5229/JECST.2015.6.2.35.

[7] G. G. Ang; Pisharath Sreekumar, Polymers as Binders and Plasticizers - Historical Perspective, Energ. Polym. - Bind. Plast. Enhancing Performance. 37 (2012) 510. doi:10.1002/prep.201280003.

[8] S. Chaturvedi, P.N. Dave, Solid propellants: AP/HTPB composite propellants, Arab. J. Chem. (2015). doi:10.1016/j.arabjc.2014.12.033.

[9] N. Bertrand, P. Colin, M. Ranger, J. Leblond, Designing Polymeric Binders for Pharmaceutical Applications, in: 2013: pp. 483–517. doi:10.1039/9781849737821-00483.

[10] P. Tourneroche, J.C. Gelin, M. Sahli, T. Barrière, Development and thermo-physical characterization of polymers/metallic powder mixtures for MIM application, Procedia Eng. 81 (2014) 2530–2536. doi:10.1016/j.proeng.2014.10.362.

[11] A. Royer, T. Barriére, J.C. Gelin, Development of bio-sourced binder to metal injection moulding, in: AIP Conf. Proc., AIP Publishing LLC, 2016: p. 020009. doi:10.1063/1.4963413.

[12] S. Vasantrao Patil, S. Laxman Ghatage, S. Shankar Navale, N. Kadar Mujawar, Natural binders in

tablet formulation, Int. J. PharmTech Res. 6 (2014) 1070–1073. https://www.researchgate.net/publication/265644099_Natural_Binders_in_Tablet_Formulation.

[13] F. Luppi, H. Cavaye, E. Dossi, Nitrated Cross-linked β-Cyclodextrin Binders Exhibiting Low Glass Transition Temperatures, Propellants, Explos. Pyrotech. (2018). doi:10.1002/prep.201800137.

[14] J. Szejtli, Introduction and General Overview of Cyclodextrin Chemistry, Chem. Rev. 98 (1998) 1743–1754. doi:10.1021/cr970022c.

[15] R. Challa, A. Ahuja, J. Ali, R.K. Khar, Cyclodextrins in drug delivery: An updated review, AAPS PharmSciTech. 6 (2005) E329–E357. doi:10.1208/pt060243.

[16] E.M.M. Del Valle, Cyclodextrins and their uses: A review, Process Biochem. 39 (2004) 1033–1046. doi:10.1016/S0032-9592(03)00258-9.

[17] R. Solaro, E. Dossi, E. Chiellini, G. Mazzanti, New Multifunctional Polymeric Materials for the Treatment of Chronic Uremia, J. Bioact. Compat. Polym. 12 (1997) 27–46. doi:10.1177/088391159701200103.

[18] Y.K. Jeong, T.W. Kwon, I. Lee, T.S. Kim, A. Coskun, J.W. Choi, Hyperbranched β-cyclodextrin polymer as an effective multidimensional binder for silicon anodes in lithium rechargeable batteries, Nano Lett. 14 (2014) 864–870. doi:10.1021/nl404237j.

[19] J. Wang, Z. Yao, C.W. Monroe, J. Yang, Y. Nuli, Carbonyl- *β* -Cyclodextrin as a Novel Binder for Sulfur Composite Cathodes in Rechargeable Lithium Batteries, Adv. Funct. Mater. 23 (2013) 1194–1201. doi:10.1002/adfm.201201847.

[20] F. Zeng, W. Wang, A. Wang, K. Yuan, Z. Jin, Y.S. Yang, Multidimensional Polycation β-Cyclodextrin Polymer as an Effective Aqueous Binder for High Sulfur Loading Cathode in Lithium-Sulfur Batteries, ACS Appl. Mater. Interfaces. 7 (2015) 26257–26265. doi:10.1021/acsami.5b08537.

[21] W. Chen, C. Wang, L. Yan, L. Huang, X. Zhu, B. Chen, H.J. Sant, X. Niu, G. Zhu, K.N. Yu, V.A.L. Roy, B.K. Gale, X. Chen, Improved polyvinylpyrrolidone microneedle arrays with non-stoichiometric cyclodextrin, J. Mater. Chem. B. 2 (2014) 1699–1705. doi:10.1039/c3tb21698e.

[22] V. Giglio, C. Sgarlata, G. Vecchio, Novel amino-cyclodextrin cross-linked oligomer as efficient carrier for anionic drugs: A spectroscopic and nanocalorimetric investigation, RSC Adv. 5 (2015) 16664–16671. doi:10.1039/c4ra16064a.

[23] R. Solaro, S. D'Antone, L. Bemporad, E. Chiellini, New Polyfunctional Derivatives of β-Cyclodextrin

Suited for the Formulation of Drug Release Systems, J. Bioact. Compat. Polym. 8 (1993) 236–250. doi:10.1177/088391159300800303.

[24] O. Radia, E. Rogalska, G. Moulay-Hassane, Preparation of meloxicamβ-cyclodextrinpolyethylene glycol 6000 ternary system: Characterization, in vitro and in vivo bioavailability, Pharm. Dev. Technol. 17 (2012) 632–637. doi:10.3109/10837450.2011.565347.

[25] Y.Y. Liu, X.D. Fan, Synthesis and characterization of pH- and temperature-sensitive hydrogel of N-isopropylacrylamide/cyclodextrin based copolymer, Polymer (Guildf). 43 (2002) 4997–5003. doi:10.1016/S0032-3861(02)00350-6.

[26] J.-T. Zhang, S.-W. Huang, J. Liu, R.-X. Zhuo, Temperature Sensitive Poly[N-isopropylacrylamide-co-(acryloyl?-cyclodextrin)] for Improved Drug Release, Macromol. Biosci. 5 (2005) 192–196. doi:10.1002/mabi.200400167.

[27] V. Bennevault, C. Huin, P. Guégan, K. Evgeniya, X.P. Qiu, F.M. Winnik, Temperature sensitive supramolecular self assembly of per-6-PEO-β-cyclodextrin and α,ω-di-(adamantylethyl)poly(N-isopropylacrylamide) in water, Soft Matter. 11 (2015) 6432–6443. doi:10.1039/c5sm01293g.

[28] J. Thiry, F. Krier, S. Ratwatte, J.M. Thomassin, C. Jerome, B. Evrard, Hot-melt extrusion as a continuous manufacturing process to form ternary cyclodextrin inclusion complexes, Eur. J. Pharm. Sci. 96 (2017) 590–597. doi:10.1016/j.ejps.2016.09.032.

[29] H. Kono, T. Nakamura, H. Hashimoto, Y. Shimizu, Characterization, molecular dynamics, and encapsulation ability of β-cyclodextrin polymers crosslinked by polyethylene glycol, Carbohydr. Polym. 128 (2015) 11–23. doi:10.1016/j.carbpol.2015.04.009.

[30] S.K. Osman, G.M. Soliman, M. Amin, A. Zaky, Self-assembling hydrogels based on B-Cyclodextrin polymer and poly (ethylene glycol) bearing hydrophobic moieties for protein delivery, Int. J. Pharm. Pharm. Sci. 6 (2014) 591–597.

[31] F. Van De Manakker, T. Vermonden, N. El Morabit, C.F. Van Nostrum, W.E. Hennink, Rheological behavior of self-assembling PEG-β-cyclodextrin/ PEG-cholesterol hydrogels, Langmuir. 24 (2008) 12559–12567. doi:10.1021/la8023748.

[32] S. Salmaso, A. Semenzato, S. Bersani, P. Matricardi, F. Rossi, P. Caliceti, Cyclodextrin/PEG based hydrogels for multi-drug delivery, Int. J. Pharm. 345 (2007) 42–50. doi:10.1016/j.ijpharm.2007.05.035.

[33] Y.G. Jia, X.X. Zhu, Self-healing supramolecular hydrogel made of polymers bearing cholic acid and

β-cyclodextrin pendants, Chem. Mater. 27 (2015) 387–393. doi:10.1021/cm5041584.

[34] F. Herbst, D. Döhler, P. Michael, W.H. Binder, Self-healing polymers via supramolecular forces, in: Macromol. Rapid Commun., Wiley-VCH Verlag GmbH & Co. KGaA, Weinheim, Germany, (2013) 203–220. doi:10.1002/marc.201200675.

[35] T.T. Nielsen, V. Wintgens, K.L. Larsen, C. Amiel, Synthesis and characterization of poly(ethylene glycol) based β-cyclodextrin polymers, J. Incl. Phenom. Macrocycl. Chem. 65 (2009) 341–348. doi:10.1007/s10847-009-9591-0.

[36] H.-J. Schneider, F. Hacket, V. Rüdiger, H. Ikeda, NMR Studies of Cyclodextrins and Cyclodextrin Complexes, Chem. Rev. 98 (1998) 1755–1786. doi:10.1021/cr970019t.

[37] T. Miao, S.L. Fenn, P.N. Charron, R.A. Oldinski, Self-Healing and Thermoresponsive Dual-Cross-Linked Alginate Hydrogels Based on Supramolecular Inclusion Complexes, Biomacromolecules. 16 (2015) 3740–3750. doi:10.1021/acs.biomac.5b00940.

[38] K. Guo, M.S. Lin, J.F. Feng, M. Pan, L.S. Ding, B.J. Li, S. Zhang, The Deeply Understanding of the Self-Healing Mechanism for Self-Healing Behavior of Supramolecular Materials Based on Cyclodextrin–Guest Interactions, Macromol. Chem. Phys. 218 (2017) 1600593. doi:10.1002/macp.201600593.

[39] H. Fujita, Y. Einaga, Self Diffusion and Viscoelasticity in Entangled Systems I. Self-Diffusion Coefficients, Polym. J. 17 (1985) 1131–1139. doi:10.1295/polymj.17.1131.

[40] M. Muthukumar, A. Baumgärtner, Diffusion of a Polymer Chain in Random Media, Macromolecules. 22 (1989) 1941–1946. doi:10.1021/ma00194a071.

[41] Y. Yang, X. Ding, M.W. Urban, Chemical and physical aspects of self-healing materials, Prog. Polym. Sci. 49–50 (2015) 34–59. doi:10.1016/j.progpolymsci.2015.06.001.

[42] X. Zhao, Multi-scale multi-mechanism design of tough hydrogels: building dissipation into stretchy networks, Soft Matter. 10 (2014) 672–687. doi:10.1039/C3SM52272E.

[43] E. Specogna, K.W. Li, M. Djabourov, F. Carn, K. Bouchemal, Dehydration, dissolution, and melting of cyclodextrin crystals, J. Phys. Chem. B. 119 (2015) 1433–1442. doi:10.1021/jp511631e.

[44] G. Zhou, T. Zhao, J. Wan, C. Liu, W. Liu, R. Wang, Predict the glass transition temperature and plasticization of β-cyclodextrin/water binary system by molecular dynamics simulation, Carbohydr. Res. 401 (2015) 89–95. doi:10.1016/j.carres.2014.10.026.

[45] C. Rodríguez-Tenreiro, C. Alvarez-Lorenzo, Á. Concheiro, J.J. Torres-Labandeira, Characterization of cyclodextrincarbopol interactions by DSC and FTIR, J. Therm. Anal. Calorim. 77 (2004) 403–411. doi:10.1023/B:JTAN.0000038981.30494.f4.

[46] S.K. Behera, D. Saha, P. Gadige, R. Bandyopadhyay, Effects of polydispersity on the glass transition dynamics of aqueous suspensions of soft spherical colloidal particles, Phys. Rev. Mater. 1 (2017) 055603. doi:10.1103/PhysRevMaterials.1.055603.

[47] S.J. Li, S.J. Xie, Y.C. Li, H.J. Qian, Z.Y. Lu, Influence of molecular-weight polydispersity on the glass transition of polymers, Phys. Rev. E. 93 (2016) 012613. doi:10.1103/PhysRevE.93.012613.

[48] B. ESCAIG, Binding metals to polymers. A short review of basic physical mechanisms, Le J. Phys. IV. 03 (1993) C7-753-C7-761. doi:10.1051/jp4:19937120.

[49] Y. Bai, L. Jin, Characterization of frequency-dependent glass transition temperature by Vogel-Fulcher relationship, J. Phys. D. Appl. Phys. 41 (2008) 152008. doi:10.1088/0022-3727/41/15/152008.

[50] G. Kister, E. Dossi, Cure monitoring of CFRP composites by dynamic mechanical analyser, Polym. Test. 47 (2015) 71–78. doi:10.1016/j.polymertesting.2015.08.009.

[51] N. Tabary, M.J. Garcia-Fernandez, F. Danède, M. Descamps, B. Martel, J.F. Willart, Determination of the glass transition temperature of cyclodextrin polymers, Carbohydr. Polym. 148 (2016) 172–180. doi:10.1016/j.carbpol.2016.04.032.

[52] M.D. Hager, P. Greil, C. Leyens, S. Van Der Zwaag, U.S. Schubert, Self-healing materials, Adv. Mater. 22 (2010) 5424–5430. doi:10.1002/adma.201003036.

[53] S.R. White, B.J. Blaiszik, S.L.B. Kramer, S.C. Olugebefola, J.S. Moore, N.R. Sottos, Self-healing polymers and composites, Am. Sci. 99 (2011) 392–399. doi:10.1179/095066010X12646898728408.

[54] A. Klaewklod, V. Tantishaiyakul, N. Hirun, T. Sangfai, L. Li, Characterization of supramolecular gels based on β-cyclodextrin and polyethyleneglycol and their potential use for topical drug delivery, Mater. Sci. Eng. C. 50 (2015) 242–250. doi:10.1016/j.msec.2015.02.018.

[55] J. Klein, Evidence for reptation in an entangled polymer melt, Nature. 271 (1978) 143–145. doi:10.1038/271143a0.

Figure captions

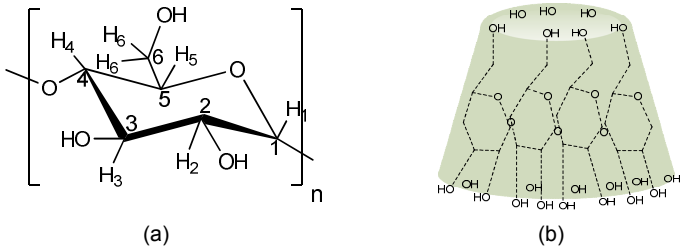

Fig. 1. a) Chemical structure of α (n=6), β (n=7) and γ (n=8) cyclodextrins. b) Toroid structure of a cyclodextrin molecule [13].

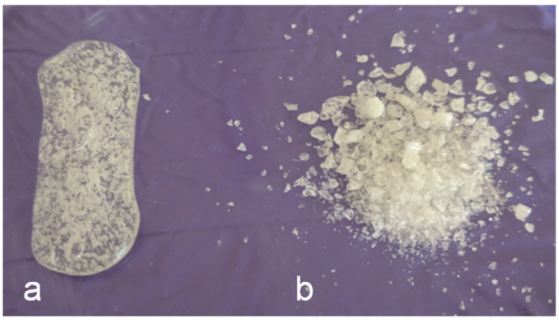

Fig. 2. Physical characteristics of βCPCD: a) malleable βCPCD1, and b) powdery βCPCD3.

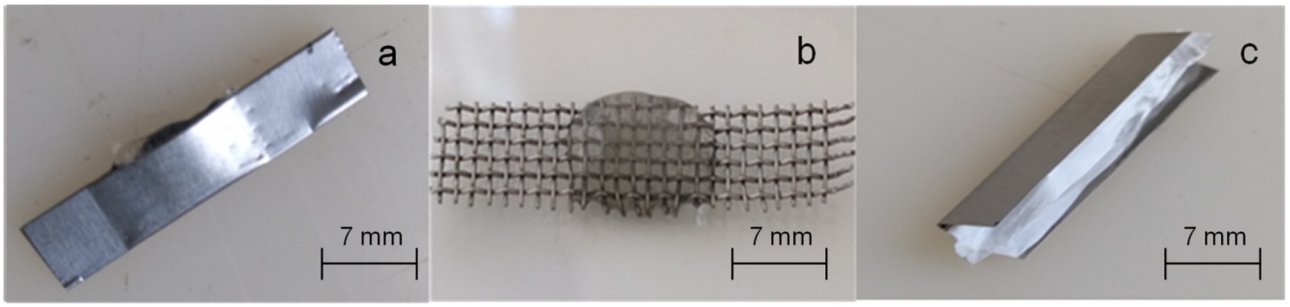

Fig. 3. Photographs of βCPCD samples supported by a) an aluminium pocket, b) a stainless-steel mesh, and c) an aluminium pocket wrapped in PTFE tape.

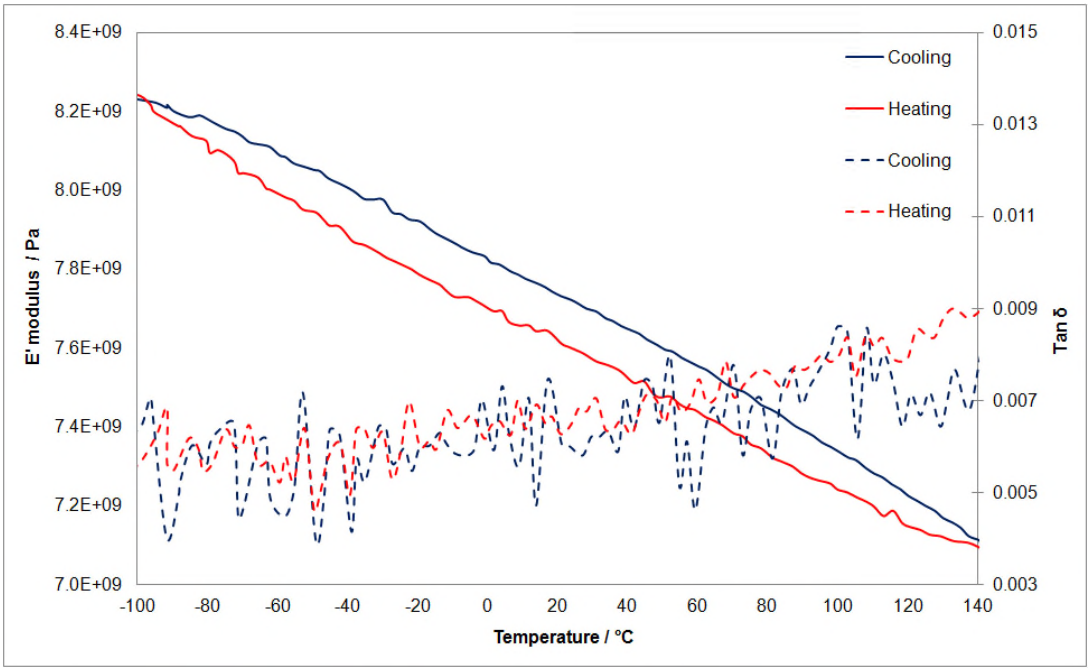

Fig. 4. Dynamic mechanical analysis showing the variation of the storage modulus (E′) (solid lines) and tanδ (dashed lines) of βCD (10 °C min^{-1}, 1 Hz, third temperature cycle from –100 °C to 140 °C, aluminium pocket).

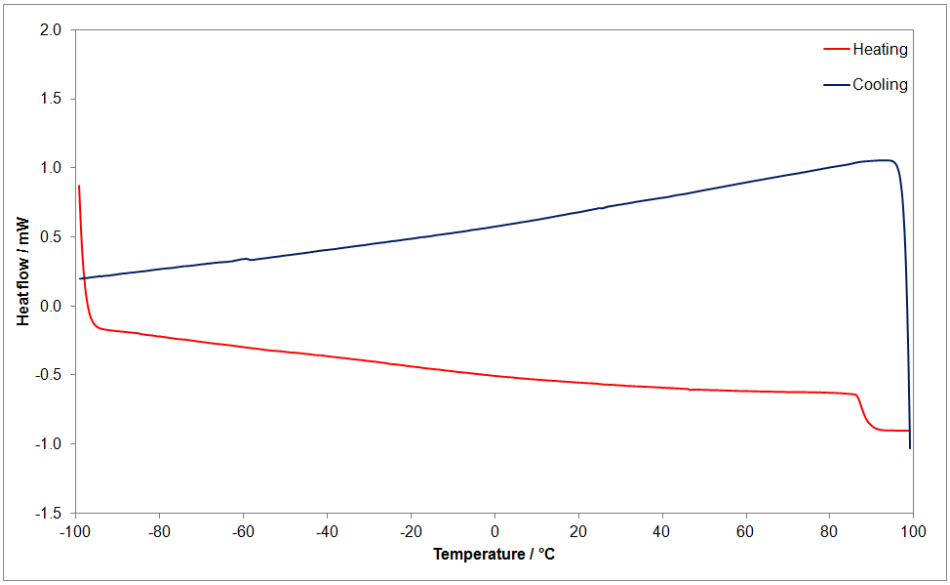

Fig. 5. Differential scanning calorimetry thermogram of βCD (10 °C min^{-1}, third temperature cycle from –100 °C to 100 °C).

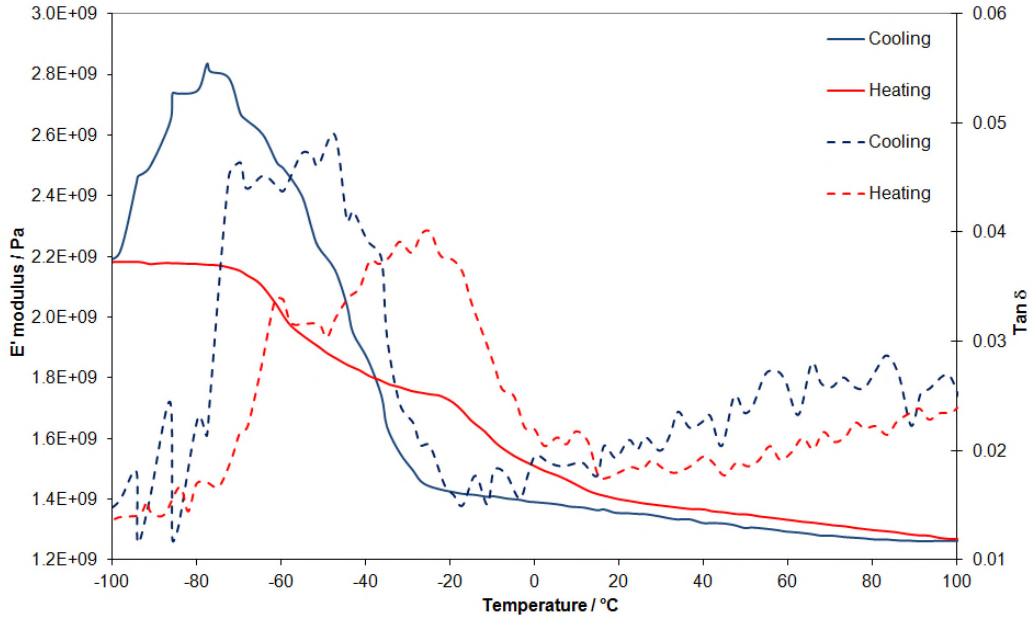

Fig. 6. Dynamic mechanical analysis showing the variation of the storage modulus (E′) (solid lines) and tanδ (dashed lines) of PEGDGE (10 °C min^{-1}, 1 Hz, third temperature cycle from –100 °C to 100 °C, aluminium pocket).

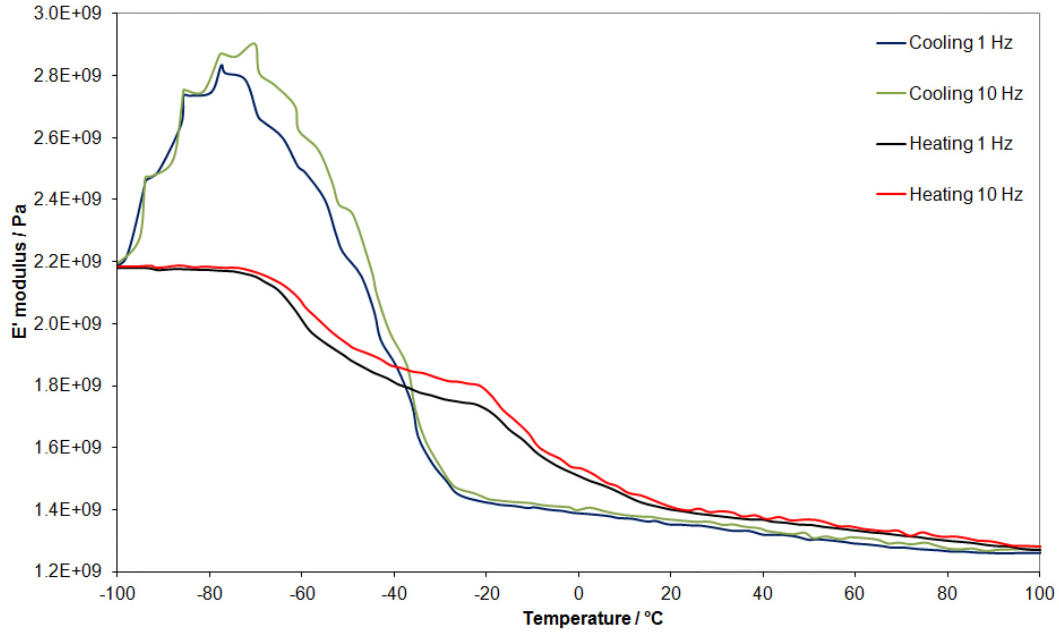

Fig. 7. Dynamic mechanical analysis showing the variation of the storage modulus (E′) of PEGDGE with frequency (1 and 10 Hz) during cooling (blue and green lines) and heating (black and red lines) (10 °C min^{-1}, third temperature cycle from –100 °C to 100 °C, aluminium pocket).

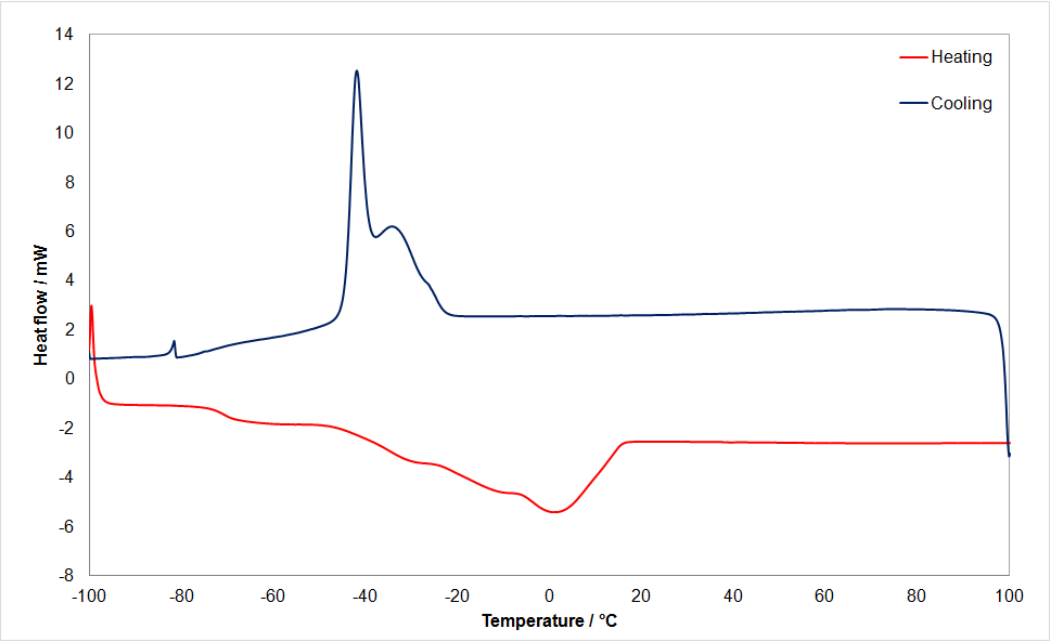

Fig. 8. Differential scanning calorimetry thermogram of PEGDGE from –100 ° to 100 °C (10 °C min^{-1}, third temperature cycle, aluminium crucible).

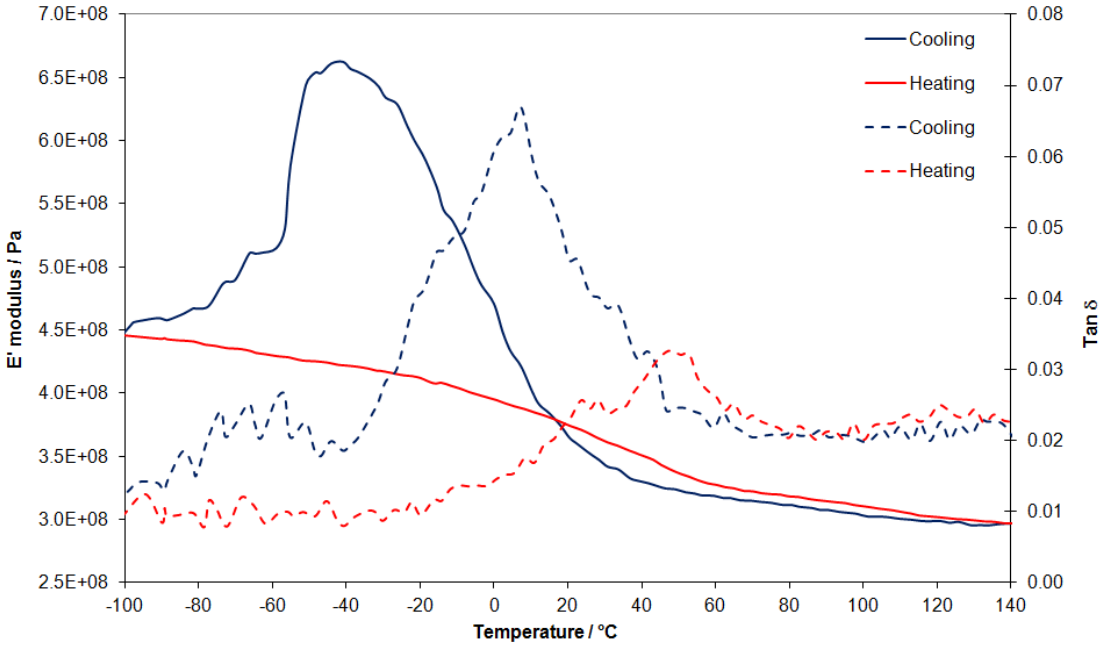

Fig. 9. Dynamic mechanical analysis showing the variation of the storage modulus (E′) (solid lines) and tanδ (dashed lines) of βCPCD1 (10 °C min^{-1}, 1 Hz, third temperature cycle from –100 °C to 140 °C, aluminium pocket).

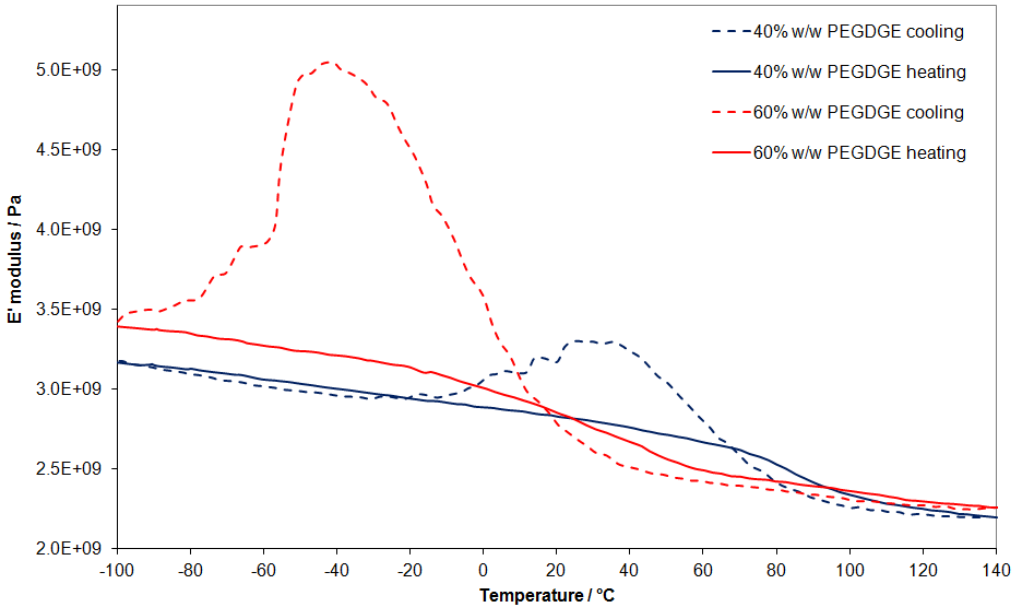

Fig. 10. Dynamic mechanical analysis showing the variation of the storage modulus (E′) and tanδ of βCPCD1 (60% w/w PEGDGE, solid and dotted red lines) and βCPCD3 (40% w/w PEGDGE, solid and dotted blue lines) (10 °C min^{-1}, 1 Hz, third temperature cycle from –100 °C to 140 °C, aluminium pocket).

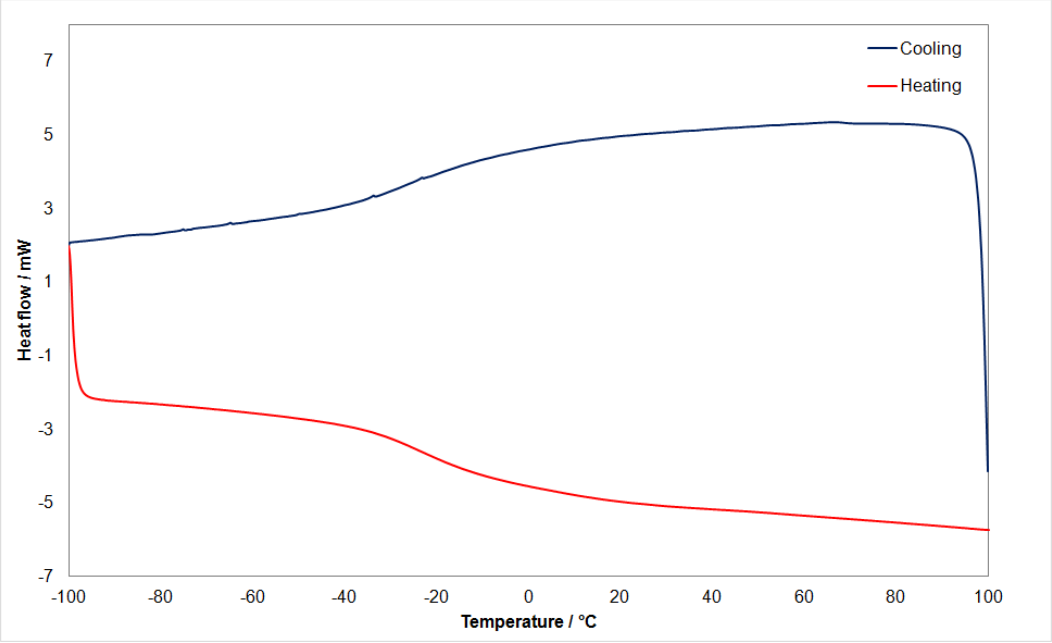

Fig. 11. Differential scanning calorimetry thermogram of βCPCD1 from –100 ° to 100 °C (10 °C min^{-1}, third temperature cycle, aluminium crucible).

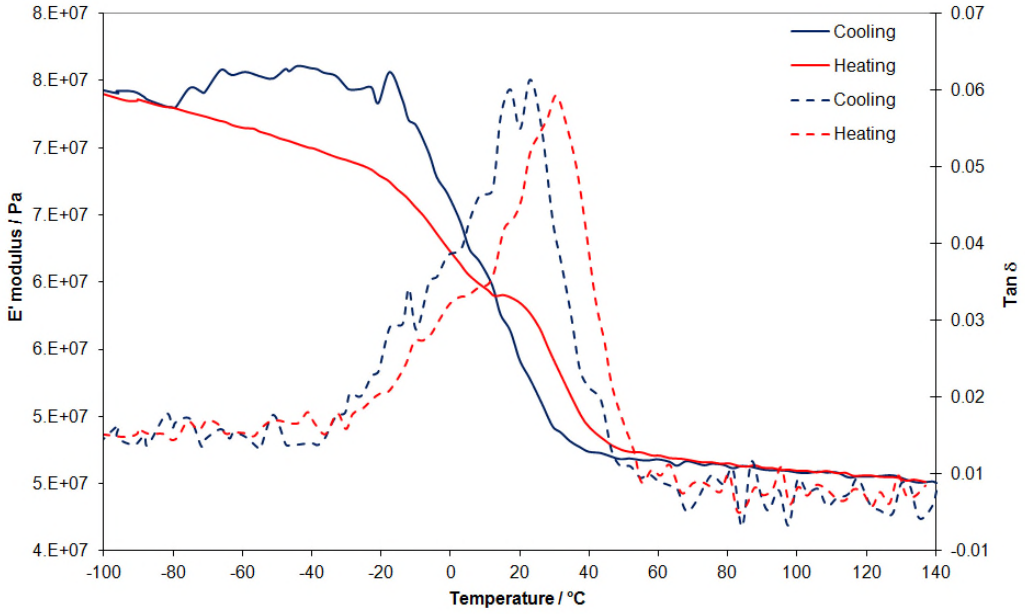

Fig. 12. Dynamic mechanical analysis showing the variation of the storage modulus (E′) (solid lines) and tanδ (dashed lines) of βCPCD1 (10 °C min^{-1}, 1 Hz, third temperature cycle from –100 °C to 140 °C, stainless-steel mesh).

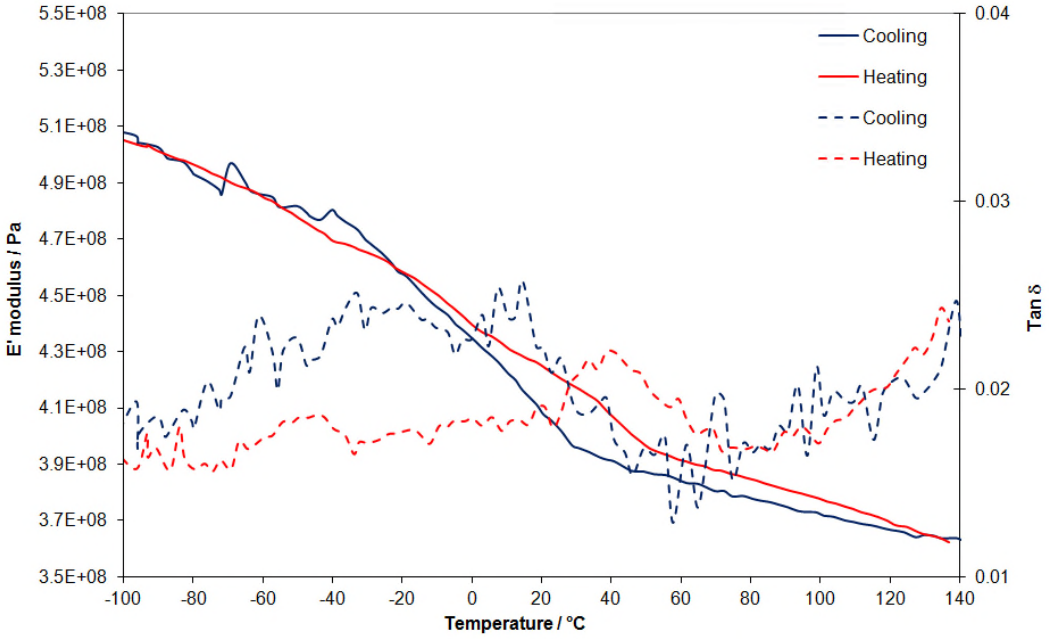

Fig. 13. Dynamic mechanical analysis showing the variation of the storage modulus (E′) (solid lines) and tanδ (dashed lines) of βCPCD1 (10 °C min^{-1}, 1 Hz, third temperature cycle from –100 °C to 140 °C, aluminium pocket and PTFE tape).

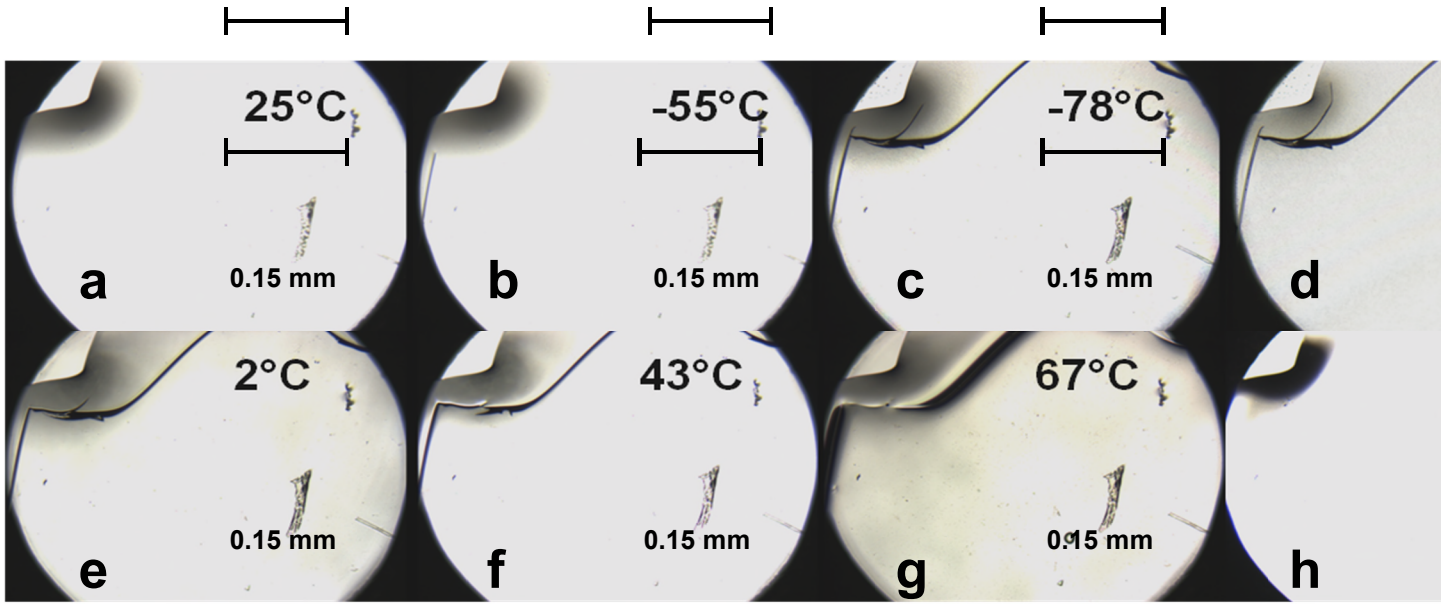

Fig. 14. Optical microscope images of βCPCD1 (60 % w/w PEGDGE) during the first temperature cycle from –100 to 100 °C. The top row (a-d) shows the cooling phase captured at 25, –55, –78 and –80 °C, and the bottom row (e-h) shows the heating phase captured at 2, 43, 67 and 87 °C .

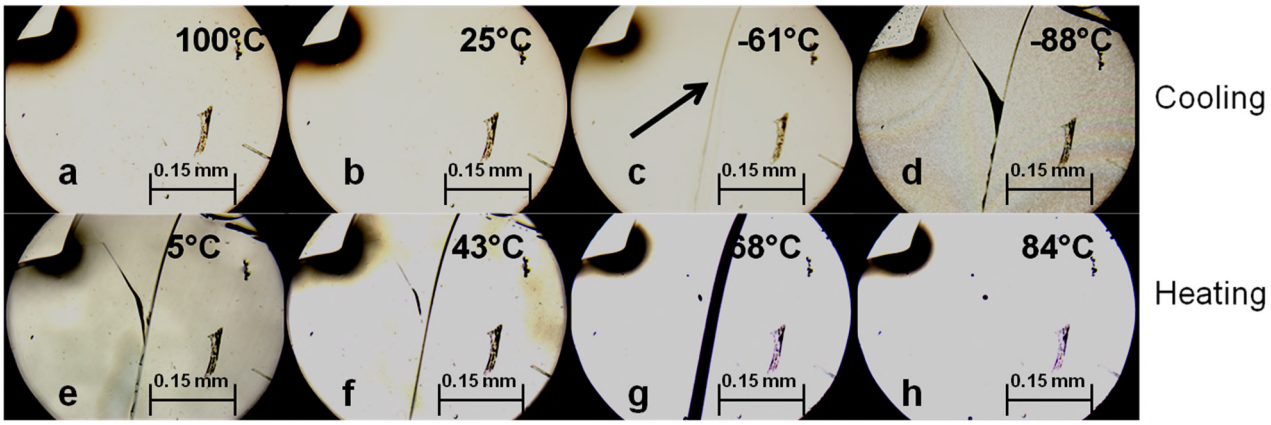

Fig. 15. Optical microscope images of βCPCD1 (60% w/w PEGDGE) during the second temperature cycle from –100 to 100°C. The top row (a-d) shows the cooling phase captured at 100, 25, –61 and –88 °C, and the bottom row (e-h) shows the heating phase captured at 5, 43, 68 and 84 °C.

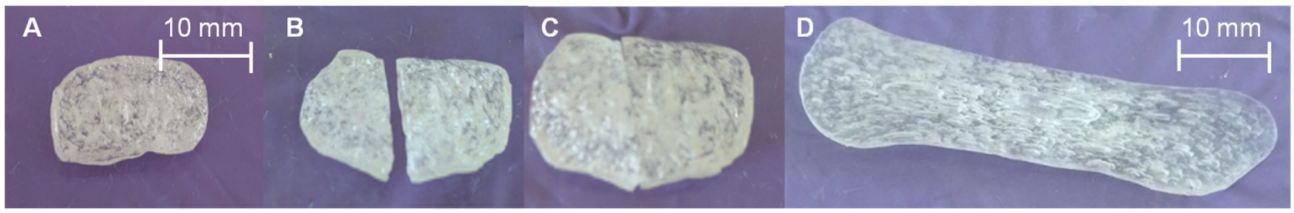

Fig. 16. Self-healing of βCPCD1 (60% w/w PEGDGE). a) Sample after solvent evaporation. b) Sample after cutting. c) The parts are placed in contact. d) The sample is heated to 70 °C for 30 min and pulled by the extremities.

Table 1

Dynamic mechanical analysis and differential scanning calorimetry data for βCPCD samples and their precursors.

Sample	PEGDGE:βCD (% w/w)	Cracking temperature[1] (°C)	E' drop (%)	T_g (°C)	
				DMA[2]	DSC[3]
βCD	-	-	-	-	83
PEGDGE	100/0	-70	23	-60/-25	-73/-41/-20[4]
βCPCD1	60-40	-42	33	41	-17
βCPCD2	55-45	-31	21	75	-8
βCPCD3	40-60	+42	11	93	+96

1 The third cooling cycle at 1 Hz
2 The tanδ peak
3 Midpoint
4 The tanδ peaks of the three major transitions of PEGDGE